LETTER

doi:10.1038/nature10154

Structure-based design of non-natural amino-acid inhibitors of amyloid fibril formation

Stuart A. Sievers[1]*, John Karanicolas[2,3]*, Howard W. Chang[1]*, Anni Zhao[1]*, Lin Jiang[1]*, Onofrio Zirafi[4], Jason T. Stevens[3], Jan Münch[4], David Baker[2] & David Eisenberg[1]

Many globular and natively disordered proteins can convert into amyloid fibrils. These fibrils are associated with numerous pathologies[1] as well as with normal cellular functions[2,3], and frequently form during protein denaturation[4,5]. Inhibitors of pathological amyloid fibril formation could be useful in the development of therapeutics, provided that the inhibitors were specific enough to avoid interfering with normal processes. Here we show that computer-aided, structure-based design can yield highly specific peptide inhibitors of amyloid formation. Using known atomic structures of segments of amyloid fibrils as templates, we have designed and characterized an all-D-amino-acid inhibitor of the fibril formation of the tau protein associated with Alzheimer's disease, and a non-natural L-amino-acid inhibitor of an amyloid fibril that enhances sexual transmission of human immunodeficiency virus. Our results indicate that peptides from structure-based designs can disrupt the fibril formation of full-length proteins, including those, such as tau protein, that lack fully ordered native structures. Because the inhibiting peptides have been designed on structures of dual-β-sheet 'steric zippers', the successful inhibition of amyloid fibril formation strengthens the hypothesis that amyloid spines contain steric zippers.

The finding that dozens of pathologies, including Alzheimer's disease, are associated with amyloid fibrils has stimulated research on fibril inhibition. One approach uses the self-associating property of proteins that form fibrils to poison fibril formation with short peptide segments[6–11]. A second approach is based on screening for molecules that can disrupt fibril formation[12,13]. Here we take a third approach to fibril inhibition: structure-based design of non-natural peptides targeted to block the ends of fibrils. With advanced sampling techniques and by minimizing an appropriate energy function, we identify novel candidate inhibitors computationally from a large peptide space that interact favourably with our template structure. This approach has been made possible by the determination of several dozen fibril-like atomic structures of segments from amyloid-forming proteins[14–16].

These structures reveal a common motif called a steric zipper, in which a pair of β-sheets is held together by the interdigitation of their side chains[14]. Using as templates the steric-zipper structures formed by segments of two pathological proteins, we have designed inhibitors that cap fibril ends. As we show, the inhibitors greatly slow the fibril formation of the parent proteins of the segments, offering a route to designed chemical interventions and supporting the hypothesis that steric zippers are the principal structural elements of these fibrils.

One of the two fibril-like steric zippers that we have chosen as a target for inhibitor design is the hexapeptide VQIVYK, residues 306–311 of the tau protein, which forms intracellular amyloid fibrils in Alzheimer's disease[17]. This segment has been shown to be important for fibril formation of the full-length protein and itself forms fibrils with biophysical properties similar to full-length tau fibrils[15,18,19]. Our second template for inhibitor design, identified by the '3D profile' algorithm[20,21], is the steric-zipper structure of the peptide segment GGVLVN from the amyloid fibril formed by ^{248}PAP^{286}, a proteolytic fragment containing residues 248–286 of prostatic acid phosphatase, a protein abundant in semen. ^{248}PAP^{286} fibrils, also known as semen-derived enhancer of virus infection (SEVI), enhance human immunodeficiency virus (HIV) infection by orders of magnitude in cell culture studies, whereas the monomeric peptide is inactive[22].

Our computational approach to designing non-natural peptides that inhibit fibril formation is summarized in Fig. 1 for the VQIVYK segment of tau protein; the same general strategy is used for the GGVLVN segment of ^{248}PAP^{286}. In both systems, we design a tight interface between the inhibiting peptide and the end of the steric zipper to block additional segments from joining the fibril. By sampling L or D amino acids, or commercially available non-natural amino acids, we can design candidate inhibitors with side chains that maximize hydrogen bonding and hydrophobic interactions across the interface.

We propose that the steric-zipper structures of the VQIVYK and GGVLVN segments represent the spines of the fibrils formed by the parent proteins containing these segments. Supporting our hypothesis are our results that D-amino-acid inhibitors designed on the VQIVYK steric-zipper template inhibit fibril formation not only of the VQIVYK segment, but also of two tau constructs, K12 and K19[23,24] (Fig. 2a). Similarly, the peptide composed of non-natural amino acids designed on the GGVLVN template inhibits the fibril formation of ^{248}PAP^{286} and greatly inhibits the HIV infectivity of human cells in culture.

To design a D-amino-acid hexapeptide sequence that interacts favourably with the VQIVYK steric zipper[15], and prevents further addition of tau molecules to the fibril, we used the Rosetta software[25]. This led to the identification of four D-amino-acid peptides: D-TLKIVW, D-TWKLVL, D-DYYFEF and D-YVIIER, in which the prefix signifies that all α-carbon atoms are in the D configuration (Fig. 2b, c, Supplementary Figs 1 and 2 and Supplementary Table 1). In the D-TLKIVW design model (Fig. 2b, c and Supplementary Fig. 1), the inhibitor packs tightly across the top of the VQIYVK steric-zipper structure, maintaining all main-chain hydrogen bonds. The side-chain hydrogen bonding between layers of stacked Gln 307 residues is replaced in the designed interface by an interaction with D-Lys 3. Several hydrophobic interactions between D-TLKIVW and the two VQIVYK β-strands contribute to the favourable binding energy (Supplementary Table 1). In the design, the D-peptide blocks the addition of another layer of VQIVYK, both above the D-peptide and across on the mating β-sheet (Supplementary Fig. 3). D-Leu 2 of the designed inhibitor prevents the addition of a VQIVYK molecule above it through a steric clash with Ile 308 of VQIVYK and on the mating sheet through a clash with Val 306 and Ile 308 (Supplementary Fig. 3). These steric clashes involving D-Leu 2 are intended to block fibril growth.

[1]Departments of Biological Chemistry and Chemistry and Biochemistry, Howard Hughes Medical Institute, UCLA, Box 951970, Los Angeles, California 90095-1570, USA. [2]Department of Biochemistry and Howard Hughes Medical Institute, University of Washington, Seattle, Washington 98195, USA. [3]Center for Bioinformatics and Department of Molecular Biosciences, University of Kansas, 1200 Sunnyside Avenue, Lawrence, Kansas 66045-7534, USA. [4]Institute of Molecular Virology, University Hospital Ulm, Meyerhofstrasse 1, 89081 Ulm, Germany.
*These authors contributed equally to this work.

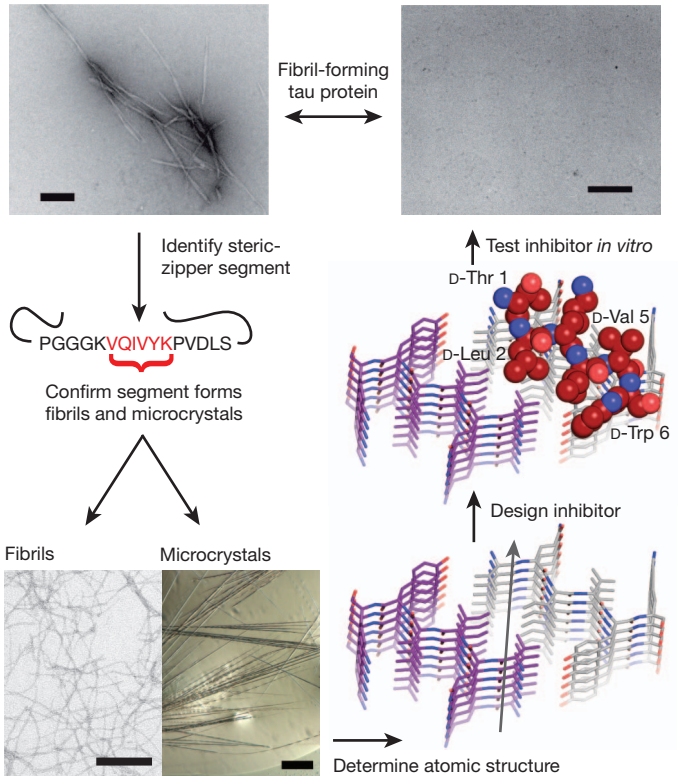

Figure 1 | Design and characterization of peptide inhibitors of amyloid fibril formation. Tau constructs form fibrils *in vitro*[24] (top left; scale bar, 200 nm). The VQIVYK segment in isolation forms fibrils and microcrystals (bottom left; fibril scale bar, 200 nm; microcrystal scale bar, 100 μm). The atomic structure of the fibril-like VQIVYK segment reveals a characteristic steric-zipper motif[15] comprising a pair of interacting β-sheets (purple and grey) running along the fibril axis (grey arrow) (bottom right). We designed a D-amino-acid peptide to bind to the end of the steric-zipper template and prevent fibril elongation (middle right). The D-peptide (red) is designed to satisfy hydrogen bonds and make favourable non-polar interactions with the molecule below, while preventing the addition of other molecules above and on the opposite β-sheet. As shown *in vitro*, the designed D-peptide prevents the formation of fibrils when incubated with tau K19 (upper right; scale bar, 200 nm).

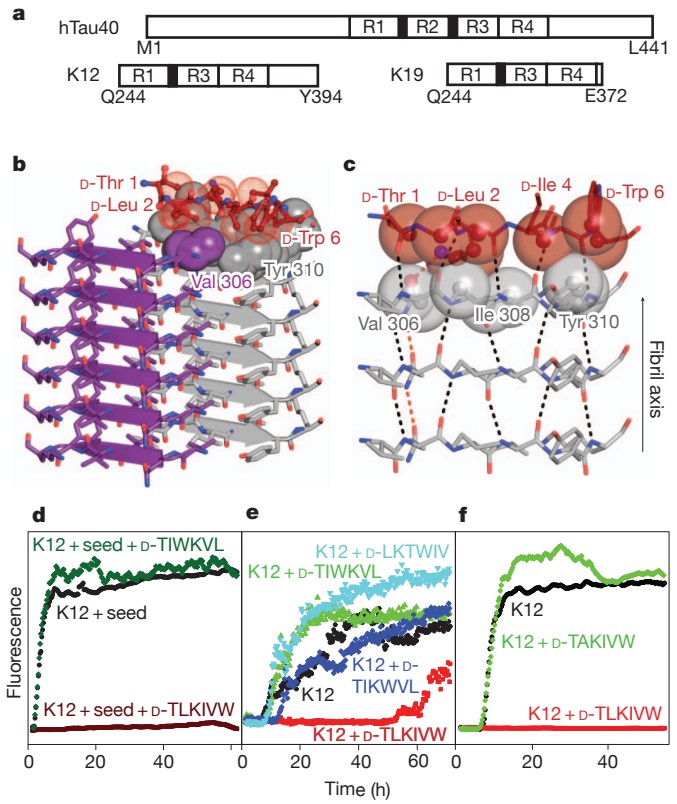

Figure 2 | Designed D-peptide delays tau K12 fibril formation in a sequence-specific manner. **a**, Tau construct composition[23]. The longest human tau isoform found in the central nervous system, hTau40 (Uniprot ID, P10636-8), contains four microtubule-binding repeats, R1 to R4, whereas K12 and K19 lack R2. The black bars at the amino termini of R2 and R3 represent the fibrillogenic segments VQIINK and VQIVYK, respectively. **b**, The inhibitor D-TLKIVW (red) is designed to interact with atoms on both β-strands of the VQIVYK steric zipper (grey) primarily through hydrophobic packing and hydrogen-bonding interactions. **c**, The inhibitor interacts with the VQIVYK β-strand below. The transparent spheres show where the two molecules interact favourably. Black and red dashes indicate main-chain and side-chain hydrogen bonds, respectively. Stereo views of **b** and **c** are shown in Supplementary Fig 1. **d**, The seeded fibril formation of 50 μM K12 in the presence and absence of a tenfold molar excess of peptide was monitored by Thioflavin S fluorescence. In the presence of the scrambled peptide D-TIWKVL (dark green) and alone (black), seeded K12 fibril formation occurs with almost no lag time. However, D-TLKIVW prevents fibril formation for days (maroon). **e**, At equimolar concentrations, D-TLKIVW (red) inhibits the fibril formation of 50 μM K12. D-TIKWVL (blue), with only three residues scrambled, shows weak inhibition. However, no inhibition is observed for either D-TIWKVL (green) or D-LKTWIV (cyan). **f**, The replacement of D-Leu 2, designed to clash with VQIVYK on the opposite sheet, with D-Ala eliminates the inhibition of fibril formation.

We used fluorescence spectroscopy and electron microscopy to assess whether the designed D-peptides inhibit the fibril formation of the tau segment VQIVYK and of the tau constructs K12 and K19. Of our designed inhibitors, D-TLKIVW is the most effective (Supplementary Fig. 4). Electron microscopy, performed after three days, verified that incubation with equimolar D-TLKIVW prevents K19 fibril formation, which would otherwise have occurred within the elapsed time (Fig. 1, upper right). D-TLKIVW delays fibril formation of VQIVYK, K12 and K19 even when present in sub-equimolar concentration (Supplementary Fig. 5). A fivefold molar excess of D-TLKIVW delays K12 fibril formation for more than two weeks in some experimental replicates (Supplementary Fig. 5c, d). In tenfold molar excess, D-TLKIVW prevents the fibril formation of K12 for more than 60 hours in the presence of preformed K12 fibril seeds, suggesting that the peptide interacts with fibrils (Fig. 2d). Also, kinetic analysis shows that the fibril elongation rate decreases in the presence of increasing concentrations of inhibitor peptide (Supplementary Fig. 6). The large increase in lag time in unseeded reactions may be due to interactions with small aggregates formed during the process of fibril formation.

To investigate the specificity of the designed inhibitor, we tested scrambled sequence variants of D-TLKIVW that have poor (that is, high) calculated energies and unfavourable packing (Supplementary Table 1). The scrambled peptides D-TIKWVL, D-TIWKVL and D-LKTWIV have little inhibitory effect when present at an equimolar ratio with VQIVYK, K12 and K19 (Fig. 2e and Supplementary Fig. 7), showing that the inhibition is sequence specific. Also, the diastereomer, L-TLKIVW, is less effective than D-TLKIVW (Supplementary Fig. 8). As a further test of the specificity of our design, we confirmed that D-TLKIVW is unable to block the fibril formation of amyloid-β, which also is associated with Alzheimer's disease (Supplementary Fig. 9). This suggests that the D-peptide inhibitor is not general to amyloid systems, but is specific to the VQIVYK interface in tau protein. Such specificity is essential for designed inhibitors if they are not to interfere with proteins that natively function in an amyloid state[3].

To confirm that the designed D-peptide inhibits in accordance with the design model (Fig. 2b, c and Supplementary Fig. 1), we performed several additional tests. First we visualized the position of the inhibitor D-TLKIVW relative to fibrils of the tau construct K19 using electron microscopy. We covalently linked Monomaleimido Nanogold particles

both to the inhibitor and, separately, to a scrambled hexapeptide, D-LKTWIV. We used a blind counting assay and found that, relative to Nanogold alone, D-TLKIVW shows a significant binding preference for the end of fibrils, in contrast to the scrambled control peptide, D-LKTWIV (Fig. 3a and Supplementary Fig. 10).

As a further test of the model, we used NMR to characterize the binding affinity of D-TLKIVW for tau fibrils. The ^{1}H NMR spectra for D-TLKIVW were collected in the presence of increasing concentrations of VQIVYK or K19 fibrils. Because neither K19 nor VQIVYK contains tryptophan, we were able to monitor the ^{1}H resonance of the indole proton of the tryptophan in our inhibitor. When bound to a fibril, the inhibitor, D-TLKIVW, is removed from the soluble phase and the ^{1}H resonance is diminished[26] (Fig. 3b and Supplementary Fig. 11). As a control, we also measured spectra for the non-inhibiting peptide D-LKTWIV present with D-TLKIVW in the same reaction mixture. As shown in Fig. 3b, the presence of VQIVYK fibrils at a given concentration reduces the D-TLKIVW indole resonance much more than it does the D-LKTWIV indole resonance. Spectra of the two peptides are shown in Supplementary Fig. 12. By monitoring the D-TLKIVW indole resonance over a range of VQIVYK fibril concentrations, we estimate the apparent dissociation constant of the interaction between D-TLKIVW and VQIVYK fibrils to be ~2 μM (Supplementary Fig. 11a and Methods). This value corresponds to a standard free binding energy of ~7.4 kcal mol^{-1}, with ~2.5 kcal mol^{-1} from non-polar interactions and ~4.9 kcal mol^{-1} from six hydrogen bonds (Methods). Repeating the NMR binding experiment with K19 fibrils yields a similar trend (Supplementary Fig. 11b). To determine whether D-TLKIVW has affinity for soluble VQIVYK, we measured ^{1}H NMR spectra of D-TLKIVW and D-LKTWIV in the presence of increasing amounts of soluble VQIVYK. Only a slight change in the respective chemical shifts of the indole proton peaks of D-TLKIVW and D-LKTWIV is observed, even at a 70-fold molar excess of VQIVYK (Supplementary Fig. 13). This, together with the ability of the peptide to prevent seeded fibril formation, suggests that D-TLKIVW does not interact with monomers but rather with a structured, fibril-like species.

As another test of our design model, we replaced the D-Leu residue with D-Ala in D-TLKIVW. Our structural model suggests that D-Leu 2 of D-TLKIVW is important for preventing tau fibril formation because of its favourable interaction with the Ile residue of the VQIVYK molecule below and with Ile and the first Val of VQIVYK across the steric zipper (Fig. 2b, c and Supplementary Fig. 1). The D-Ala replacement eliminates these interactions and, furthermore, removes a steric clash that would occur were another VQIVYK molecule placed across from the inhibitor (Supplementary Fig. 3 and Supplementary Table 1). When the D-Ala variant is incubated with VQIVYK and the tau constructs, it has no inhibitory effect on fibril formation (Fig. 2f and Supplementary Fig. 14). This confirms that D-Leu 2 is critical for the efficacy of D-TLKIVW, consistent with our model.

In summary, although our electron microscopy, NMR and D-Ala replacement results support a model in which the designed peptide D-TLKIVW binds to the ends of tau fibrils, they do not constitute proof that the inhibitors bind exactly as anticipated in the designs (Supplementary Fig. 15).

To expand on our design methodology, we computationally designed an inhibitor of ^{248}PAP^{286} fibril formation containing non-natural L-amino acids (Fig. 4b and Supplementary Fig. 16), using the GGVLVN structure as a template (Fig. 4a and Supplementary Table 2). This peptide, Trp-His-Lys-chAla-Trp-hydroxyTic (WW61), contains an Ala derivative, β-cyclohexyl-L-alanine (chAla) and a Tyr/Pro derivative, 7-hydroxy-(*S*)-1,2,3,4-tetrahydroisoquinoline-3-carboxylic acid (hydroxyTic), both of which increase contact area with the GGVLVN template. The non-natural chAla forms hydrophobic interactions with the Leu residue in the steric-zipper interface, and hydroxyTic supports the favourable placement of chAla through hydrophobic packing (Fig. 4b and Supplementary Fig. 16b).

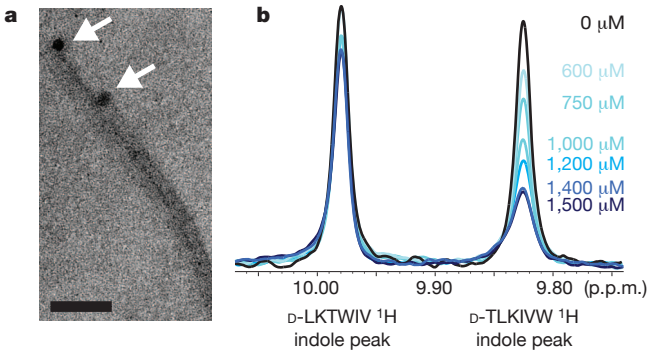

Figure 3 | Mechanism of interaction. **a**, Nanogold covalently bound to D-TLKIVW localizes at the ends (arrows) of two tau K19 fibrils. Scale bar, 50 nm. **b**, The inhibitor D-TLKIVW binds to fibrils with an estimated affinity constant in the low micromolar range, as shown by the indole proton region of the 500-MHz ^{1}H NMR spectra of D-TLKIVW (9.83 p.p.m.) and D-LKTWIV (9.98 p.p.m.) in the presence of increasing concentrations of VQIVYK fibrils. The resonance of the D-TLKIVW indole proton is reduced in the presence of increasing concentrations of VQIVYK fibrils, whereas the indole proton signal for the scrambled control peptide D-LKTWIV is only slightly affected. Fibril solutions contained 0–1,500 μM VQIVYK monomers, as indicated.

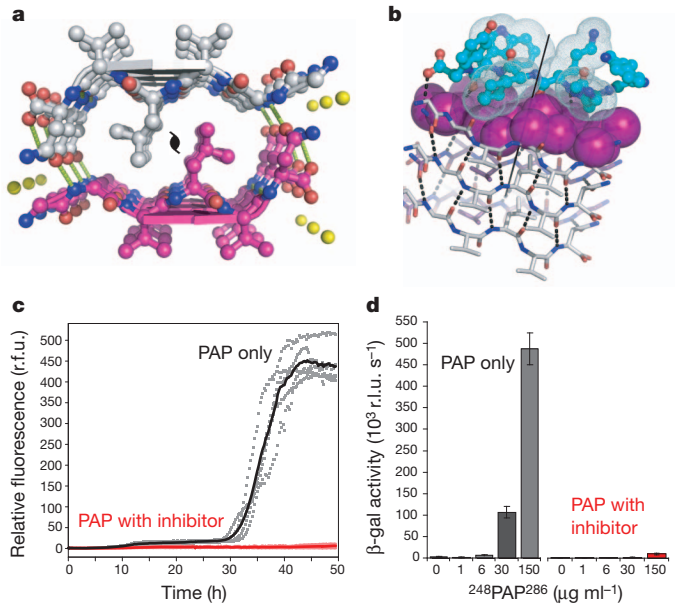

Figure 4 | Designed non-natural peptide inhibits ^{248}PAP^{286} fibril formation. **a**, The view down the fibril axis of the crystal structure of the GGVLVN steric zipper reveals two mating β-sheets with parallel, in-register β-strands (hydrogen bonds, green dashed lines; water molecules, yellow spheres). **b**, View roughly perpendicular to a fibril of three layers, with the atoms of the side chains of the top layer shown as purple spheres. On top is a designed non-natural peptide inhibitor, Trp-His-Lys-chAla-Trp-hydroxyTic (blue; see Supplementary Fig. 16). **c**, The inhibitor blocks ^{248}PAP^{286} fibril formation, as shown by monitoring Thioflavin T fluorescence. With a twofold molar excess of the inhibitor (pale red), the fluorescence remains low over the course of the experiment for all five replicates, unlike in the absence of inhibitor (grey). Mean fluorescence values are shown as solid red and black lines with and without the inhibitor, respectively. r.f.u., relative fluorescence units. **d**, HIV infection rates were determined by monitoring β-galactosidase (β-gal) activity. Agitated ^{248}PAP^{286} alone efficiently increases viral infection, whereas ^{248}PAP^{286} mixtures incubated with inhibitor were unable to enhance HIV infection. Peptide concentrations during virion treatment are indicated on the *x* axis. Error bars show the s.d. of three measurements per sample. r.l.u., relative light units.

Moreover, we propose that the bulky side chains and steric constraints of hydroxyTic provide hindrance to further fibril growth.

This designed peptide, WW61, effectively delays both seeded and unseeded fibril formation of ^{248}PAP^{286} *in vitro* (Fig. 4c and Supplementary Figs 17 and 18). In the presence of a twofold molar excess of this inhibitor, seeded fibril formation is efficiently blocked for more than two days (Fig. 4c). Furthermore, we see that increasing the concentration of this inhibitor extends the fibril formation lag time (Supplementary Fig. 19). These inhibition assay results were further confirmed by electron microscopy (Supplementary Fig. 20). As a control for specificity, we tested the effect of GIHKQK, from the amino terminus of ^{248}PAP^{286}, and PYKLWN, a peptide with the same charge as WW61. Neither peptide affected fibril formation kinetics, indicating that the inhibitory activity of the designed peptide is sequence specific (Supplementary Fig. 21).

Because ^{248}PAP^{286} fibrils (SEVI) have been shown to enhance HIV infection[22], using a functional assay we investigated whether WW61 is able to prevent this enhancement. In this experiment, we treated HIV particles with ^{248}PAP^{286} solutions that had been agitated for 20 hours (to allow fibril formation) in the presence or absence of WW61, and infected TZM-bl indicator cells. As has been previously observed, SEVI efficiently enhanced HIV infection[22]. However, ^{248}PAP^{286} incubated with the designed inhibitor prevented HIV infection (Fig. 4d).

We performed several control experiments to verify that the lack of infectivity observed in the assay is indeed due to the inhibition of SEVI formation. First we confirmed that in the absence of SEVI the designed inhibitor WW61 does not affect HIV infectivity (Supplementary Fig. 22a). We also found that the control peptides GIHKQK and PYKLWN, which do not inhibit ^{248}PAP^{286} fibril formation, fail to decrease HIV infectivity (Supplementary Fig. 22b). Additionally, we observed that WW61 has no inhibitory effect on polylysine-mediated HIV infectivity[27], further ruling out a non-specific electrostatic interaction mechanism (Supplementary Fig. 22a). Together, these results demonstrate that a peptide capable of preventing ^{248}PAP^{286} fibril formation also inhibits the generation of virus-enhancing material.

Structure-based design of inhibitors of amyloid fibril formation has been challenging in the absence of detailed information about the atomic-level interactions that form the fibril spine. So far, one of the most successful structure-based approaches to preventing fibril formation has been to stabilize the native tetrameric structure of transthyretin[28]. That approach is well suited to the prevention of fibril formation of proteins with known native structures, but other proteins involved in amyloid-related diseases, such as tau protein, amyloid-β and ^{248}PAP^{286}, lack fully ordered native structures[29]. Our structure-based approach makes it possible to design inhibitors independent of native structure. Instead, the templates are atomic-level structures of short, fibril-forming segments[14,15]. By using these fibril-like templates, and adopting computational methods successful in designing novel proteins and protein–protein interfaces[25,30], we have created specific inhibitors of proteins that normally form fibrils. These results support the hypothesis that the steric zipper is a principal feature of tau-related and SEVI fibrils, and suggest that, with current computational methods and steric-zipper structures, we have the tools to design specific inhibitors to prevent the formation of other amyloid fibrils.

METHODS SUMMARY

We used crystal structures of hexapeptide segments of VQIVYK and GGVLVN as templates to design peptide inhibitors using the Rosetta software[25]. Briefly, this algorithm searches possible side-chain conformations (called rotamers) of all amino acids in a peptide β-strand backbone stacked onto the fibril end of both segment structures. The Rosetta software is extended to sample the approximate side-chain conformation of non-natural D and L amino acids by adapting side-chain torsion angles from those in their natural counterparts. The lowest energy set of side-chain rotamers is identified by combinatorial optimization of a potential consisting of a term for the Lennard–Jones potential, an orientation-dependent hydrogen-bond potential term, an implicit solvation term and a structure-derived side-chain and backbone torsional potential term.

Full Methods and any associated references are available in the online version of the paper at www.nature.com/nature.

Received 6 December 2010; accepted 21 April 2011.
Published online 15 June 2011.

1. Westermark, P. *et al.* A primer of amyloid nomenclature. *Amyloid* **14,** 179–183 (2007).
2. Maji, S. K. *et al.* Functional amyloids as natural storage of peptide hormones in pituitary secretory granules. *Science* **325,** 328–332 (2009).
3. Fowler, D. M., Koulov, A. V., Balch, W. E. & Kelly, J. W. Functional amyloid – from bacteria to humans. *Trends Biochem. Sci.* **32,** 217–224 (2007).
4. Astbury, W. T. & Dickinson, S. The X-ray interpretation of denaturation and the structure of the seed globulins. *Biochem. J.* **29,** 2351–2360 (1935).
5. Calamai, M., Chiti, F. & Dobson, C. M. Amyloid fibril formation can proceed from different conformations of a partially unfolded protein. *Biophys. J.* **89,** 4201–4210 (2005).
6. Tjernberg, L. O. *et al.* Arrest of β-amyloid fibril formation by a pentapeptide ligand. *J. Biol. Chem.* **271,** 8545–8548 (1996).
7. Findeis, M. A. Peptide inhibitors of β amyloid aggregation. *Curr. Top. Med. Chem.* **2,** 417–423 (2002).
8. Sciarretta, K. L., Gordon, D. J. & Meredith, S. C. Peptide-based inhibitors of amyloid assembly. *Methods Enzymol.* **413,** 273–312 (2006).
9. Soto, C., Kindy, M. S., Baumann, M. & Frangione, B. Inhibition of Alzheimer's amyloidosis by peptides that prevent β-sheet conformation. *Biochem. Biophys. Res. Commun.* **226,** 672–680 (1996).
10. Kokkoni, N., Stott, K., Amijee, H., Mason, J. M. & Doig, A. J. *N*-methylated peptide inhibitors of amyloid aggregation and toxicity. Optimization of the inhibitor structure. *Biochemistry* **45,** 9906–9918 (2006).
11. Sato, T. *et al.* Inhibitors of amyloid toxicity based on β-sheet packing of Aβ40 and Aβ42. *Biochemistry* **45,** 5503–5516 (2006).
12. Larbig, G., Pickhardt, M., Lloyd, D. G., Schmidt, B. & Mandelkow, E. Screening for inhibitors of tau protein aggregation into Alzheimer paired helical filaments: a ligand based approach results in successful scaffold hopping. *Curr. Alzheimer Res.* **4,** 315–323 (2007).
13. Wiesehan, K. *et al.* Selection of D-amino-acid peptides that bind to Alzheimer's disease amyloid peptide $a\beta_{1-42}$ by mirror image phage display. *ChemBioChem* **4,** 748–753 (2003).
14. Nelson, R. *et al.* Structure of the cross-β spine of amyloid-like fibrils. *Nature* **435,** 773–778 (2005).
15. Sawaya, M. R. *et al.* Atomic structures of amyloid cross-β spines reveal varied steric zippers. *Nature* **447,** 453–457 (2007).
16. Wiltzius, J. J. *et al.* Molecular mechanisms for protein-encoded inheritance. *Nature Struct. Mol. Biol.* **16,** 973–978 (2009).
17. Selkoe, D. J. Alzheimer's disease: genes, proteins, and therapy. *Physiol. Rev.* **81,** 741–766 (2001).
18. Goux, W. J. *et al.* The formation of straight and twisted filaments from short tau peptides. *J. Biol. Chem.* **279,** 26868–26875 (2004).
19. von Bergen, M. *et al.* Assembly of τ protein into Alzheimer paired helical filaments depends on a local sequence motif (^{306}VQIVYK^{311}) forming β structure. *Proc. Natl Acad. Sci. USA* **97,** 5129–5134 (2000).
20. Goldschmidt, L., Teng, P. K., Riek, R. & Eisenberg, D. Identifying the amylome, proteins capable of forming amyloid-like fibrils. *Proc. Natl Acad. Sci. USA* **107,** 3487–3492 (2010).
21. Thompson, M. J. *et al.* The 3D profile method for identifying fibril-forming segments of proteins. *Proc. Natl Acad. Sci. USA* **103,** 4074–4078 (2006).
22. Münch, J. *et al.* Semen-derived amyloid fibrils drastically enhance HIV infection. *Cell* **131,** 1059–1071 (2007).
23. Friedhoff, P., von Bergen, M., Mandelkow, E. M., Davies, P. & Mandelkow, E. A nucleated assembly mechanism of Alzheimer paired helical filaments. *Proc. Natl Acad. Sci. USA* **95,** 15712–15717 (1998).
24. Wille, H., Drewes, G., Biernat, J., Mandelkow, E. M. & Mandelkow, E. Alzheimer-like paired helical filaments and antiparallel dimers formed from microtubule-associated protein tau *in vitro*. *J. Cell Biol.* **118,** 573–584 (1992).
25. Kuhlman, B. *et al.* Design of a novel globular protein fold with atomic-level accuracy. *Science* **302,** 1364–1368 (2003).
26. Chen, Z., Krause, G. & Reif, B. Structure and orientation of peptide inhibitors bound to β-amyloid fibrils. *J. Mol. Biol.* **354,** 760–776 (2005).
27. Roan, N. R. *et al.* The cationic properties of SEVI underlie its ability to enhance human immunodeficiency virus infection. *J. Virol.* **83,** 73–80 (2009).
28. Petrassi, H. M., Klabunde, T., Sacchettini, J. & Kelly, J. W. Structure-based design of *N*-phenyl phenoxazine transthyretin amyloid fibril inhibitors. *J. Am. Chem. Soc.* **122,** 2178–2192 (2000).
29. Schweers, O., Schonbrunn-Hanebeck, E., Marx, A. & Mandelkow, E. Structural studies of tau protein and Alzheimer paired helical filaments show no evidence for β-structure. *J. Biol. Chem.* **269,** 24290–24297 (1994).
30. Fleishman, S. J. *et al.* Computational design of proteins targeting the conserved stem region of influenza hemagglutinin. *Science* **332,** 816–821 (2011).

Supplementary Information is linked to the online version of the paper at www.nature.com/nature.

Acknowledgements We thank M. I. Ivanova, J. Corn, T. Kortemme, D. Anderson, M. R. Sawaya, M. Phillips, S. Sambashivan, J. Park, M. Landau, A. Laganowsky, Q. Zhang, R. Clubb, F. Guo, T. Yeates, J. Nowick, J. Zheng and M. J. Thompson for discussions; the HHMI, NIH, NSF, Gates Foundation and Joint Center for Translational Medicine for support; R. Peterson for help with NMR experiments; E. Mandelkow for providing tau constructs; R. Riek for providing amyloid-β; and J. Stroud for amyloid-β preparation.

Support came from the Damon Runyon Cancer Research Foundation (J.K.), the Ruth L. Kirschstein National Research Service Award (H.W.C.), the programme for junior professors by the Ministry of Science, Baden-Württemberg (J.M.), and a UCLA-IGERT bioinformatics traineeship (S.A.S.).

Author Contributions S.A.S., J.K., D.B., J.M. and D.E. designed the project. J.K. and S.A.S. created the design protocol. J.K. designed the D-peptides. L.J. expanded the design methodology and designed the non-natural amino-acid peptides. S.A.S., H.W.C. and A.Z. performed the fluorescence experiments and electron microscopy, and analysed kinetic data. A.Z. determined the structure of GGVLVN. O.Z. performed the HIV infectivity experiments. J.T.S. determined the tau fibril elongation rates. S.A.S. performed the NMR experiments. S.A.S., J.K. and D.E. wrote the manuscript and coordinated contributions by other authors.

Author Information Atomic coordinates and structure factors for the reported GGVLVN structure have been deposited in the Protein Data Bank with accession code 3PPD. Reprints and permissions information is available at www.nature.com/reprints. The authors declare no competing financial interests. Readers are welcome to comment on the online version of this article at www.nature.com/nature. Correspondence and requests for materials should be addressed to D.E. (david@mbi.ucla.edu).

METHODS

Computational design. Computational designs were carried out using the Rosetta software[25] (http://www.rosettacommons.org). This algorithm involves building side-chain rotamers of all amino acids onto a fixed protein backbone. The lowest energy set of side-chain rotamers is then identified as those which minimize an energy function containing a Lennard–Jones potential, an orientation-dependent hydrogen-bond potential, a solvation term, amino-acid-dependent reference energies and a statistical torsional potential that depends on the backbone and side-chain dihedral angles.

D-amino-acid tau inhibitors. The crystal structure of VQIVYK (ref. 15; Protein Data Bank ID, 2ON9) was used as a starting scaffold for computational design. To take full advantage of the statistical nature of the rotamer library and some terms in the Rosetta energy function, the stereochemistry of the fibril scaffold was inverted so that design would take place using L amino acids. An extended L-peptide was aligned with the N, C and O backbone atoms of the D-fibril scaffold. This L-peptide was subsequently redesigned, keeping all atoms of the D-fibril fixed. The stereochemistry of the final design model was then inverted, yielding a D-peptide designed to cap an L-fibril. We inspected the finished models to confirm that inversion of the stereochemistry at the Thr and Ile Cβ atoms did not make the designs energetically unfavourable. Energetic consequences of incorporating a D inhibitor peptide in the middle of an L fibril were subsequently evaluated to ensure that fibril propagation could not continue after association of an inhibitor. Calculations of the area buried and shape complementarity were performed with AREAIMOL[31] and SC[32], respectively.

L-peptide ^{248}PAP^{286} inhibitors. The crystal structure of GGVLVN (PDB ID, 3PPD) was used as a template for the following design procedure. An extended L-peptide was aligned according to crystal symmetry. Small, random perturbations of the L-peptide were performed to optimize the rigid-body arrangement between the fibril template and the peptide inhibitor. Full sequence optimization of the inhibitor was performed using the Rosetta software package, allowing residues directly contacting the inhibitor to repack; other scaffold residues remained fixed. Because the design calculations use a discrete rotamer representation of the side chains, we next performed simultaneous quasi-Newtonian optimization of the inhibitor rigid-body orientation, the side-chain torsion angles and, in some cases, the backbone torsion angles using the full-atom Rosetta energy function. This optimization was essential to the subsequent assessment of the inhibition of the design. Several iterative runs of small perturbations in inhibitor placement, interface design and refinement were performed to improve hydrogen-bonding and packing interactions. The designs that ranked highest on the basis of the total binding energy between the inhibitor and the fibril scaffold and the interfacial shape complementarity[32] were subsequently synthesized and tested.

For each initial active L-peptide design, the non-natural L amino acids were incorporated using a growth strategy. Non-natural amino acids, structurally similar to those of initial active designs, were selected on the basis of their solubility, side-chain shape and commercial availability. Side-chain conformations were approximately sampled by adopting side-chain torsion angles from those in their natural counterparts. Sequence optimization of the inhibitor was performed and the optimal set of rotamers identified using Monte Carlo simulated annealing with the full-atom energy function described above. The resulting designs were ranked on the basis of the total binding energy between the inhibitor and the fibril scaffold.

Tau construct expression and purification. pNG2 expression vectors (derived from pET-3b[33]) containing either the K12 or K19 gene were provided by E. Mandelkow[34]. Expression in BL21(DE3) *Escherichia coli*[33] was induced with 1 mM isopropyl thiogalactoside when the absorbance $A_{600\,nm}$ was between 0.8 and 1.0, and cells were collected after 3–4 h. K12 and K19 were purified on the basis of previously described methods[35]. Cells were pelleted for 20 min at 4,700*g* and resuspended in 20 mM MES, pH 6.8, 1 mM EDTA, 0.2 mM $MgCl_2$, 5 mM DTT, 1 mM PMSF and a protease inhibitor cocktail. The cells were sonicated for 2.5 min and, following addition of NaCl to bring cell lysate to 0.5 M NaCl, the lysate was boiled for 20 min. The lysate was sedimented at 30,000*g* for 20 min and dialyzed twice against 20 mM MES, pH 6.8, 50 mM NaCl, 1 mM EDTA, 1 mM $MgCl_2$, 2 mM DTT and 0.1 mM PMSF at 4 °C. The dialysate was pelleted for 20 min at 30,000*g* and filtered before cation exchange chromatography on an AKTA Explorer (GE Pharmacia) with a HighTrap HP SP 5-ml column (GE Healthcare). The sample was eluted with a linear gradient of up to 60% buffer B (20 mM MES, pH 6.8, 1 M NaCl, 1 mM EDTA, 1 mM $MgCl_2$, 2 mM DTT and 0.1 mM PMSF). Size exclusion chromatography was optionally performed with a Superdex 75 10/300 GL column (GE Healthcare) in PBS buffer (137 mM NaCl, 3 mM KCl, 10 mM Na_2HPO_4, 2 mM KH_2PO_4, pH 7.4) with 1 mM DTT on the AKTA Explorer depending on preparation purity as assessed by SDS polyacrylamide gel electrophoresis.

Tau construct inhibition assays. Fibril formation assays were performed on the basis of previously published protocols[35–38]. Reaction mixtures (150 µl) containing 50 µM tau K12 or K19, as determined by the Micro BCA Protein Assay Kit (Pierce), were incubated in 250 mM sodium phosphate buffer, pH 7.4, with 1 mM DTT, 12.5 µM heparin (average molecular mass, 6,000 Da; Sigma) and 10 µM Thioflavin S (ThS; MP Bio). Inhibitor peptides (CS Bio, Celtek Biosciences) were dissolved in 250 mM phosphate buffer, pH 7.4, to 0.5 mM and added at specified molar ratios. Reactions were split into a minimum of three replicates in black, 96-well, optically clear plates (Nunc), sealed with Corning pressure-sensitive sealing tape and monitored using either a Varioskan plate reader (Thermo Scientific), for K12, or a SpectraMax M5, for K19. The fluorescence signal was measured every 15 min with excitation and emission wavelengths of 440 and 510 nm, respectively, at 37 °C, with continuous shaking at 900 r.p.m. with a diameter of 1 mm for K12, and with quiescent incubation with shaking 2 s before each reading for K19. Plots showing the fluorescence trace of the replicate with median lag time for each sample were created using R[39]. Plots of lag time depict the mean time value at which each replicate crossed an arbitrary fluorescence value above noise background (values were selected per experiment and applied to all samples). Error bars represent the standard deviation of the replicate lag times for each sample.

Seeded K12 fibril formation assays. Seeds were produced by incubating 50 µM K12 as above, but without ThS present, and were added at 0.25% (v/v). Peptide stock concentrations were 0.75 mM and were added at a final concentration of tenfold molar excess relative to soluble K12. Reaction mixtures were otherwise prepared and monitored as above.

VQIVYK inhibition assays. The VQIVYK fibril formation assay was modified from a previously published protocol[40]. Buffers and plates were kept on ice to delay VQIVYK fibril formation while the reaction mixtures were prepared. Replicate solutions of 180 µl of 25 mM MOPS, pH 7.2, 100 µM ThS and inhibitor peptides were added to black, clear-bottomed, 96-well Nunc plates with 1/8-inch PTFE beads (Orange Products). Acetylated and amidated VQIVYK (Genscript) was dissolved in H_2O to 1.3 mM and filtered through a Millipore Microcon 100-kDa filter device at 14,000*g* for 5 min at 4 °C to remove large aggregates (final concentration, ~1 mM). Filtered VQIVYK (20 µl) was added to each reaction well. ThS fluorescence was monitored at room temperature every 2 min using a SpectraMax M5 fluorometer with 2 s of mixing before each reading.

Amyloid-β fibril formation assay. Lyophilized amyloid-β(1–42) was diluted to 0.2 mg ml^{-1} in 50 mM NH_4OH and filtered with a 0.2-µm filter. The reaction mixture contained a final concentration of 11.5 µM amyloid-β(1–42), 10 µM Thioflavin T (ThT), 23 mM NH_4OH in 100 mM bicine, pH 9.1, and 11.5 µM D-TLKIVW in reactions with peptide present. Reactions were split into four replicates and the ThT fluorescence signal was measured every minute (excitation wavelength, 440 nm; emission wavelength, 510 nm), at 37 °C, with continuous shaking at 960 r.p.m. with a 1-mm diameter in a Varioskan fluorometer.

Electron microscopy. Sample (5 µl) was applied to glow-discharged, 400-mesh carbon-coated, formvar films on copper grids (Ted Pella) for 3 min. Grids were rinsed twice with distilled water and stained with 1% uranyl acetate for 90 s. Grids were examined in a Hitachi H-7000 transmission electron microscope at 75 keV or a JEOL JEM1200-EX operating at 80 keV.

Tau fibril formation kinetic analysis. The nucleation (k_1) and propagation (k_2) rates were determined by fitting the form of the Finke–Watzky two-step mechanism[41]. Plateau values were determined and the remaining parameters were fitted using the 'leasqr' nonlinear least-squares regression function (http://fly.isti.cnr.it/pub/software/octave/leasqr/) through the OCTAVE software package (http://www.gnu.org/software/octave/).

Preparation of peptide–gold conjugates. Peptide–Nanogold conjugates were prepared as described earlier for similarly sized peptides[42]. Briefly, 60 nmol of the peptides CGGG-(D)-TLKIVW and CGGG-(D)-LKTWIV (CS Bio) were dissolved in 110 µl of phosphate-buffered saline (20 mM, pH 6.5, 0.15 M NaCl), added to 6 nmol of Monomaleimido Nanogold (Nanoprobes), dissolved in 200 µl H_2O and incubated for 1 h at room temperature (22 °C) with constant rotation. Peptide–Nanogold conjugates were separated from excess unbound peptides by membrane centrifugation (Microcon-10 system, Amicon) using a molecular mass cut-off of 10 kDa. Peptide–Nanogold conjugates were then diluted into phosphate-buffered saline, aliquoted and stored at −20 °C for no longer than one month.

Preparation of K19 fibrils. K19 fibrils were generated by incubating 100 µM soluble K19 with 25 µM 6-kDa heparin overnight at 37 °C in phosphate buffer (50 mM, pH 7.4). K19 fibrils were sonicated for 15 s, using a microtip set to 35% amplitude. Residual heparin and small oligomers were removed by centrifuging the mixture through a 100-kDa Microcon concentrator for 10 min at 14,000*g*, washing the retentate with phosphate buffer and repeating three times; the retentate was restored to its original volume with phosphate buffer. These short fibril segments were stored at 4 °C for no longer than one week. For NMR studies, fibril samples were similarly prepared, but were washed in H_2O and concentrated to 2 mM K19 (by monomer).

Preparation of samples for Nanogold binding experiments. Nanogold conjugated inhibitor (or control) (10 nM) was incubated with 1.67 μM K19 fibrils (by monomer) in MOPS buffer (25 mM, pH 7.2) for 1 h. We applied 5 μl of it to a glow-discharged, 400-mesh carbon-stabilized copper grid (Ted Pella) for 3 min. The grids were washed twice with H_2O and 10 μl of the Goldenhance reagent was applied for 10 s. The grids were washed five times with H_2O and negatively stained with 2% uranyl acetate.

Quantification and localization of Nanogold binding. For each sample, 75 Nanogold particles ≤15 nm in diameter were counted and classified as bound or unbound. The 15-nm cut-off was chosen to exclude unbound, but adjacent, particles enlarged by Goldenhance that only apparently bind fibrils. To establish the localization of the binding observed, individual Nanogold particles bound to fibrils were categorized as bound to the fibril end or side. In both of these experiments, sample identities were concealed from the microscopist to ensure unbiased counting. Grids were examined with a JEOL JEM1200-EX and images were recorded using DIGITALMICROGRAPH (Gatan).

Statistical analysis of Nanogold binding. We compared counts of Nanogold-conjugated peptides and unconjugated Nanogold bound to fibrils or localizing to fibril ends. Twenty-one unconjugated Nanogold particles out of 75 counted bound to fibrils. We modelled Nanogold particles bound to fibrils using a binomial distribution with parameters $n = 75$ (sample size: number of observations) and $P = 0.28$ (probability of success). In a separate experiment, 22 unconjugated Nanogold particles bound to fibrils that localized to fibril ends, following a binomial distribution with $n = 105$ and $P = 0.21$.

Because the number of counts is fairly large, we assumed a normal distribution and used a standard Z-test to compare the number of bound Nanogold–peptide conjugates with the expected distribution based on the number of bound, unconjugated Nanogold particles. We used an analogous analysis to determine the significance of localization to fibril ends.

The numbers of Nanogold–D-TLKIVW conjugates bound to fibrils ($x_{bound} = 43$, $n = 75$) and bound Nanogold–D-TLKIVW conjugates localizing to the end of fibrils ($x_{end} = 49$, $n = 86$) were significantly different from the corresponding numbers for Nanogold alone, whereas the number of Nanogold–D-LKTWIV conjugates bound ($x_{bound} = 15$, $n = 75$) or the number localized to fibril ends ($x_{end} = 17$, $n = 100$) did not differ significantly from the corresponding numbers for Nanogold alone.

VQIVYK preparation for binding studies. Acetylated and amidated VQIVYK peptide (Genscript) was dissolved to 1 mM in 25 mM MOPS, pH 7.2, and incubated at room temperature for at least 24 h. Fibrils were washed with H_2O, concentrated using an Amicon ultracentrifugal filter with a 3-kDa molecular mass cut-off and resuspended in H_2O to a final concentration (by monomer) of 4 mM. Soluble VQIVYK was prepared by dissolving VQIVYK peptide (CS Bio) with free amino and carboxy termini in H_2O.

^{1}H NMR sample preparation and measurements. NMR samples were prepared with 5% D_2O and 10 mM NaOAc, pH 5.0. D-peptides were added from 1 mM stocks in H_2O to a final concentration of 100 μM. Soluble and fibrillar VQIVYK and tau protein were added at indicated concentrations to make a final volume of 550 μl. ^{1}H NMR spectra measured at 500 MHz were collected on a Bruker DRX500 at 283 K. H_2O resonance was suppressed through presaturation. Spectra were processed with XWINNMR 3.6.

Binding constant estimations. NMR data were analysed to estimate a binding constant for the interaction between D-TLKIVW and VQIVYK fibrils. At about 1,000 μM VQIVYK (concentration as monomer), 50% of D-TLKIVW is bound (Supplementary Fig. 11). The steric-zipper model suggests that there are two monomers per 4.7 Å (0.47-nm) layer in a fibril[14]—such that the number of monomers per fibril is given by [fibril length (nm)] × (2 monomers per 0.47 nm)—and we estimate the fibril concentration using the monomer concentration: $[VQIVYK_{fibril}] = [VQIVYK_{momomer}]/$(monomers per fibril). If we assume one binding site and estimate from electron microscopy an average length of ~140 nm per fibril, then there are about 600 monomers per fibril, and the apparent dissociation constant is about 2 μM.

Hydrogen-bonding energy calculation. We used AREAIMOL[31] to calculate the non-polar and polar areas buried by the interaction between D-TLKIVW with the VQIVYK steric zipper (Fig. 2b, c and Supplementary Fig. 1). We calculate buried areas of 201, 24 and 102 Å^2 for carbon, nitrogen and oxygen atoms, respectively. Using the atomic solvation parameters of ref. 43, we estimate that the free energy of transferring the inhibitor from a non-polar phase to an aqueous phase, $\Delta G_{solvation}$, is approximately 2.5 kcal mol^{-1}. On the basis of an apparent dissociation constant of 2 μM, we estimate the total free energy change of bringing the inhibitor into contact with the VQIVYK steric-zipper template, $\Delta G_{binding}$, to be 7.4 kcal mol^{-1}. From the interaction model (Fig. 2c and Supplementary Fig. 1), we maintain six hydrogen bonds between D-TLKIVW and VQIVYK, and estimate the free energy change per hydrogen bond to be $(\Delta G_{binding} - \Delta G_{solvation})/6$, or ~0.8 kcal mol^{-1}.

GGVLVN crystallization and structure determination. The GGVLVN peptide was dissolved in 10 mM Tris, pH 9, at 1.8 mg ml^{-1} and crystallized in 10% (w/v) PEG-8000, 0.1 M MES, pH 6.0, and 0.2 M $Zn(OAc)_2$. X-ray diffraction data was collected at APS beamline 24-ID-E. Phases were determined by molecular replacement using an idealized β-strand in PHASER[44]. Crystallographic refinement was performed using REFMAC[45]. Model building was performed with COOT[46] and illustrated with PYMOL[47].

^{248}PAP^{286} fibril formation and inhibition. Fmoc-β-cyclohexyl-L-alanine and Fmoc-7-hydroxy-(*S*)-1,2,3,4-tetrahydroisoquinoline-3-carboxylic acid were purchased from AnaSpec and the inhibitor peptide Trp-His-Lys-chAla-Trp-hydroxyTic (WW61) was synthesized by Celtek Biosciences. ^{248}PAP^{286} and WW61 were dissolved as ×1.25 and ×5 stocks in PBS, respectively, and filtered with a 0.1-μm filter. ^{248}PAP^{286} was diluted with PBS to 0.66 mM and ThT was added to 10 μM final concentration. Samples were optionally mixed with 1.32 mM WW61 and vortexed. Five replicates of 150 μl were immediately dispensed into a 96-well plate. In dose–response experiments, WW61 final concentrations were 0.33, 0.66 and 1.32 mM. Plates were continuously agitated at 960 r.p.m. at 37 °C, and ThT fluorescence readings were recorded (excitation wavelength, 440 nm; emission wavelength, 482 nm) at 15-min intervals with a Varioskan Flash fluorometer. Lag time was determined when fluorescence crossed an arbitrary value (3 r.f.u.) above background.

Effect of WW61 on fibril-mediated enhancement of HIV-1 infection. The CCR5 tropic molecular HIV-1 clone NL4_3/92TH014-2[48] was generated by transient transfection of 293T cells with proviral DNA. Supernatants were collected 48 h later and p24 concentrations determined by ELISA. TZM-bl reporter cells encoding a *lacZ* gene under the control of the viral LTR promoter were obtained through the NIH AIDS Research and Reference Reagent Program and provided by Dr John C. Kappes, Dr Xiaoyun Wu and Tranzyme[49]. HIV-1 (40 μl) containing 0.1 ng of p24 antigen was incubated with 40-μl dilutions of mixtures of ^{248}PAP^{286} and inhibitory peptide, WW61, that was either freshly prepared or had been agitated for 23 h. Peptide concentrations and experimental conditions during agitation were similar to those described above. Thereafter, 20 μl of the mixtures were used to infect 180 μl of TZM-bl cells seeded the day before (10^5 per well). Two days later, infection rates were determined by quantifying β-galactosidase activities in cellular lysates using the Gal-Screen assay (Applied Biosystems, T1027). Luminescence was recorded on an Orion microplate luminometer as relative light units per second.

Effect of WW61 on polylysine-mediated enhancement of HIV-1 infection. Polylysine (Sigma Aldrich) (50 μl) was mixed with an equal volume of WW61. Thereafter, 35-μl fivefold dilutions of the polylysine–WW61 mixture or polylysine alone were incubated with the same volume of virus and incubated for 5 min at room temperature. Polylysine–WW61 concentrations were 100, 20, 4, 0.8, 0.16, 0.032, 0.064 and 0 μg ml^{-1} during pre-incubation with virus stocks. Thereafter, 20 μl of each mixture was added to 180 μl of TZM-bl cells. The infection rate was determined two days later as described above.

Effect of WW61, GIHKQK and PYKLWN on HIV-1 infection. Each peptide (40 μl) was incubated with an equal volume of virus containing 1 ng of p24 antigens for 5 min at room temperature. Peptide concentrations were 150, 30, 6, 1.2 and 0 μg ml^{-1} during pre-incubation with virus stocks. Thereafter, 20 μl of each mixture was added separately to 180 μl of TZM-bl cells (tenfold dilution) and the infection rate was determined as above.

31. Collaborative Computational Project, Number 4. The *CCP4* suite: programs for protein crystallography. *Acta Crystallogr. D* **50,** 760–763 (1994).
32. Lawrence, M. C. & Colman, P. M. Shape complementarity at protein/protein interfaces. *J. Mol. Biol.* **234,** 946–950 (1993).
33. Studier, F. W., Rosenberg, A. H., Dunn, J. J. & Dubendorff, J. W. Use of T7 RNA polymerase to direct expression of cloned genes. *Methods Enzymol.* **185,** 60–89 (1990).
34. Biernat, J. *et al.* The switch of tau protein to an Alzheimer-like state includes the phosphorylation of two serine-proline motifs upstream of the microtubule binding region. *EMBO J.* **11,** 1593–1597 (1992).
35. Barghorn, S., Biernat, J. & Mandelkow, E. Purification of recombinant tau protein and preparation of Alzheimer-paired helical filaments in vitro. *Methods Mol. Biol.* **299,** 35–51 (2005).
36. Friedhoff, P., Schneider, A., Mandelkow, E. M. & Mandelkow, E. Rapid assembly of Alzheimer-like paired helical filaments from microtubule-associated protein tau monitored by fluorescence in solution. *Biochemistry* **37,** 10223–10230 (1998).
37. Pérez, M., Valpuesta, J. M., Medina, M., Montejo de Garcini, E. & Avila, J. Polymerization of tau into filaments in the presence of heparin: the minimal sequence required for tau-tau interaction. *J. Neurochem.* **67,** 1183–1190 (1996).
38. Schweers, O., Mandelkow, E. M., Biernat, J. & Mandelkow, E. Oxidation of cysteine-322 in the repeat domain of microtubule-associated protein tau controls the in vitro assembly of paired helical filaments. *Proc. Natl Acad. Sci. USA* **92,** 8463–8467 (1995).

39. R Development Core Team. *R: A Language and Environment for Statistical Computing* (R Foundation for Statistical Computing, Vienna) ⟨http://www.r-project.org⟩ (2008).
40. Rojas Quijano, F. A., Morrow, D., Wise, B. M., Brancia, F. L. & Goux, W. J. Prediction of nucleating sequences from amyloidogenic propensities of tau-related peptides. *Biochemistry* **45,** 4638–4652 (2006).
41. Morris, A. M., Watzky, M. A., Agar, J. N. & Finke, R. G. Fitting neurological protein aggregation kinetic data via a 2-step, minimal ''Ockham's razor'' model: the Finke-Watzky mechanism of nucleation followed by autocatalytic surface growth. *Biochemistry* **47,** 2413–2427 (2008).
42. Schmidt, K., Segond von Banchet, G. & Heppelmann, B. Labelling of peptides with 1.4-nm gold particles to demonstrate their binding sites in the rat spinal cord. *J. Neurosci. Methods* **87,** 195–200 (1999).
43. Eisenberg, D., Wesson, M. & Yamashita, M. Interpretation of protein folding and binding with atomic solvation parameters. *Chem. Scr.* **29A,** 217–221 (1989).
44. McCoy, A. J. *et al.* Phaser crystallographic software. *J. Appl. Crystallogr.* **40,** 658–674 (2007).
45. Murshudov, G. N., Vagin, A. A. & Dodson, E. J. Refinement of macromolecular structures by the maximum-likelihood method. *Acta Crystallogr. D* **53,** 240–255 (1997).
46. Emsley, P. & Cowtan, K. Coot: model-building tools for molecular graphics. *Acta Crystallogr. D* **60,** 2126–2132 (2004).
47. DeLano, W. L. *PyMOL Molecular Viewer* ⟨http://www.pymol.org⟩ (2002).
48. Papkalla, A., Munch, J., Otto, C. & Kirchhoff, F. Nef enhances human immunodeficiency virus type 1 infectivity and replication independently of viral coreceptor tropism. *J. Virol.* **76,** 8455–8459 (2002).
49. Platt, E. J., Wehrly, K., Kuhmann, S. E., Chesebro, B. & Kabat, D. Effects of CCR5 and CD4 cell surface concentrations on infections by macrophagetropic isolates of human immunodeficiency virus type 1. *J. Virol.* **72,** 2855–2864 (1998).